Scripta Materialia xxx (2015) xxx–xxx

Contents lists available at ScienceDirect

Scripta Materialia

journal homepage: www.elsevier.com/locate/scriptamat

Influence of nanovoids on α–α′ phase separation in FeCrAl oxide dispersion strengthened alloy

C. Capdevila [a,*], M.M. Aranda [a], R. Rementeria [a], R. Domínguez-Reyes [b], E. Urones-Garrote [c], M.K. Miller [d]

[a] Materalia Research Group, Centro Nacional de Investigaciones Metalúrgicas (CENIM-CSIC), Avda. Gregorio del Amo, 8, 28040 Madrid, Spain
[b] Departamento de Física, Universidad Carlos III de Madrid, 28911 Leganés, Spain
[c] Centro Nacional de Microscopía Electrónica (CNME), Universidad Complutense de Madrid, Avda. Complutense s/n, 28040 Madrid, Spain
[d] Oak Ridge National Laboratory, PO Box 2008, Oak Ridge, TN 37831-6139, USA

ARTICLE INFO

Article history:
Received 11 May 2015
Revised 28 July 2015
Accepted 29 July 2015
Available online xxxx

Keywords:
Phase separation
Ferrous alloy
Tomography
Positron annihilation spectroscopy
Spinodal decomposition

ABSTRACT

The presence of nanovoids in the vicinity of oxide particles in FeCrAl oxide dispersion strengthened (ODS) alloy has been identified. These nanovoids are inherent to the manufacturing route and remain quite resistant during heat treatments. Positron annihilation spectroscopy (PAS) experiments demonstrate that these nanovoids trap Cr inside thereby reducing the Cr-content in the matrix. This might lead to a delay in the α–α′ phase separation process as observed by atom probe tomography (APT).

The high-chromium (9–12 wt.% Cr) ferritic/martensitic steels are being considered for use in advanced nuclear systems due to their high creep rupture strength and excellent swelling resistance. However, in fossil-fired power plants the use of ferritic/martensitic steels is limited due to their low thermal creep-rupture strength at temperatures above 823 K. One way suggested to increase this limit to higher temperatures and maintain the advantages inherent in ferritic/martensitic steels (i.e. high thermal conductivity, low thermal expansion coefficient, and low void swelling during neutron irradiation relative to alternate heat resistant structural materials) is to use oxide dispersion strengthened (ODS) steels. Elevated temperature strength in these steels is obtained through microstructures that contain a high density of nanometric in size Y_2O_3 particles dispersed in a ferrite matrix. However, commercial manufacturing of these ODS alloys requires a mechanical alloying route followed by consolidation by hot extrusion, rolling, or hot isostatic pressing (HIPing). This complicated processing route induces an elevated density of nanovoids [1], and columnar grain microstructure with a strong texture that may degrade the mechanical performance. An equiaxed grain structure is required for fuel element cladding application so as to obtain good biaxial creep strength and ductility in the tubes.

The strong requirements for the new GEN-IV nuclear energy systems in terms of corrosion resistance, more precisely in the case of sodium fast reactors, have led to the development of new 13–18 wt.% Cr ODS ferritic steels [2], and even to the consideration of Al as an alloying addition. Applications of these new ODS ferritic steels are foreseen in the fields of fast reactor fuel cladding applications [3]. However, these alloys face a severe embrittlement problem because their service temperature lies in the range of 573–773 K. In this temperature range, the response of the material to extreme conditions is partly determined by α (Fe-rich) – α′ (Cr-enriched) phase separation. For this reason, Fe–Cr steels are at the center of much basic research, both experimental and numerical [4,5]. The goal of this paper is to study the effect that nanovoids generated during processing have on the α–α′ phase separation process in a high-chromium ODS ferritic steel.

The alloy selected for this study was an oxide dispersion-strengthened (ODS) steel commercially manufactured by Plansee GmbH (PM 2000™) and had a composition of 18.5 at.% Cr, 10.5% Al, 0.58% Ti, 0.23% Y, 0.28% O, 0.17% C and 0.022% N in at.%. PM 2000™ is manufactured by a mechanical alloying (MA) process in a hydrogen atmosphere, as described elsewhere [6]. Immediately after the mechanical alloying process, the powders have a grain size, which can be as fine as 1–2 nm locally [7]. This is hardly surprising given the extent of the deformation during mechanical alloying, with true strains of the order of $\varepsilon = 9$, equivalent to stretching a unit length by a factor of 8000. The

* Corresponding author.
E-mail address: ccm@cenim.csic.es (C. Capdevila).

http://dx.doi.org/10.1016/j.scriptamat.2015.07.044
1359-6462/

consolidation process involves hot extrusion and rolling at ~1273 K, which causes dynamic recrystallization into a sub-micrometer grain size [8,9]. With the aim of achieving a chemically homogeneous material compared with the as-hot rolled, a high temperature annealing treatment for recrystallization of 1623 K for 3 h was performed (ReX samples).

Transmission electron microscopy (TEM) was performed on 3-mm diameter discs mechanically thinned to a thickness of ~100 μm, and subsequently electropolished in a TENUPOL device at 266 K with an applied current of 40 V and an electrolyte of 5% perchloric acid, 25% glycerol, and 70% ethanol. TEM examination was performed in a JEOL JEM-3000 F microscope operating at 300 keV with a point-to-point resolution of 0.17 nm, and equipped with a high-angle annular dark-field (HAADF) detector. The STEM HAADF images were obtained with an inner collection semi-angle of 62 mrad.

The void microstructure resulting from the fabrication process of ODS alloys was studied according with the procedure reported by De Castro et al. [10] and Parish and Miller [11], by changing the focus of the high-resolution TEM images in order to locate the nanovoids and enhance their visibility. It is worth mentioning that, even after homogenization annealing at 1623 K, the presence of nanovoids was detected in the microstructure. The nanovoids were mainly distributed within the grains and were frequently observed attached to the oxide particles as well as at dislocations and grain boundaries, which were present in PM2000™. A HR-TEM image showing nanovoids in the matrix of PM2000™ are shown in Fig. 1(a). The nanovoids appear lighter than the background, which is the contrast normally observed for voids larger than ~5 nm in in-focus images. In comparison, a HAADF-STEM image of another region, Fig. 1(b), showing features with a darker contrast than the matrix. The contrast in HAADF images depends on the atomic number Z, and consequently nanovoids as well as oxides embedded in the matrix would all be imaged with a darker contrast than the surrounding matrix. It would be concluded from Fig. 1 that void size is ~4 nm. Finally, some authors reports that some nanovoids, likely those not associated to particles, becomes unstable and annealed out at 1323 K, whereas those associated with particles remain stable after annealing at 1523 K [12]. However, our observations confirm the presence of nanovoids that are not clearly associated to oxide particles after homogenization annealing at 1623 K.

Also, there exist other PAS results in non-ODS Fe12Cr and Fe14Cr processed by PM route that reveal the formation of nanovoids and/or tridimensional vacancy clusters [13].

The α–α' phase separation process was analyzed during ageing treatment at 748 K for several times by atom probe tomography (APT). Needle-shaped specimens for APT were cut from bulk material and electropolished with the use of the standard double layer and micropolishing methods [14]. APT analyses were performed with the ORNL local electrode atom probe (LEAP®). The CAMECA Instruments LEAP 2017 was operated in voltage-pulsed mode with a specimen temperature of 60 K, a pulse repetition rate of 200 kHz, and a pulse fraction of 0.2.

Because α–α' phase separation is a diffusion driven process, its kinetics should be boosted if the number density of vacancies increases. Therefore, subsequent heat treatments at 1473 K for 5 min followed by a rapid quench to room temperature (ANN samples), after homogenization annealing at 1623 K, were performed in order to increase the number density of vacancies to promote the α–α' phase separation process.

The three-dimensional microstructure, as determined by APT, resulting from aging at 748 K, is shown in Fig. 2. Because of the relatively low chromium content of the alloy, the Cr-enriched α' phase is in the form of isolated particles rather than the interconnected network structure observed previously in Fe-24–45% Cr alloys [15]. The kinetics of the α–α' phase separation was quantitatively determined by analyzing the evolution of the composition amplitude (ΔC). The composition amplitude was determined from the phase compositions derived from proximity histograms [16]. The evolutions of ΔC with aging time, t, at 748 K for the ReX and ANN samples are shown in Fig. 3. The kinetics of the α–α' phase separation are illustrated by the variation of ΔC with ageing time for both conditions analyzed. It is clear the faster kinetics observed in the ReX samples as compared with ANN samples. As a general comment, it is concluded from Fig. 3 that the variation of ΔC follows a $\sim t^{1/3}$ dependence, which is consistent with a power law dependent growth of the mean precipitate size $R(t)$ varying as $\approx t^{1/3}$ predicted by Lifshitz–Slyozov–Wagner (LSW) theory [17,18]. Nevertheless, one would expect a faster kinetics for α–α' phase separation in ANN samples due to the higher density of point defects (vacancies) and dislocations that enhance the diffusion driven processes. However, the opposite behavior is derived from

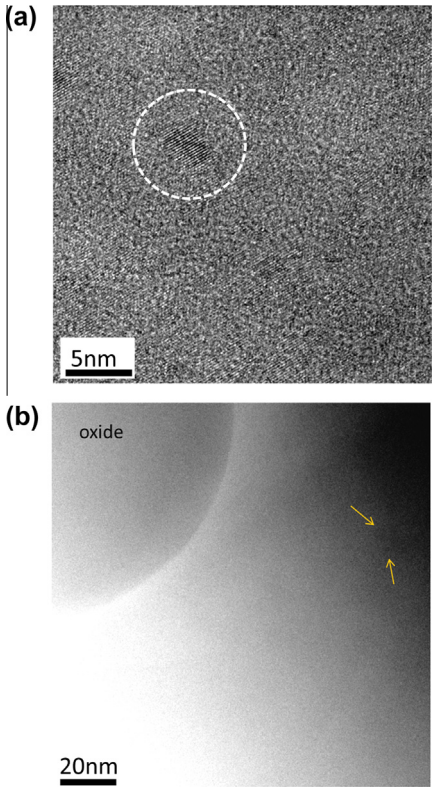

Fig. 1. (a) HR-TEM image showing nanovoids in the matrix of PM2000. (b) HAADF-STEM image of nanovoids close to an oxide particle that present a darker contrast than the matrix.

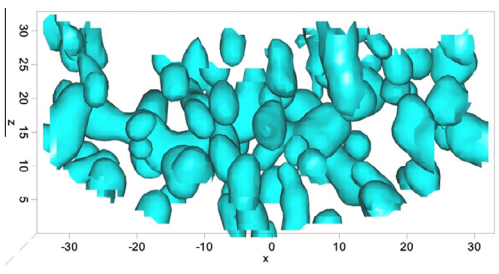

Fig. 2. 30% Cr isoconcentration surface illustrating the three-dimensional microstructure in ANN sample after ageing for 3800 h at 748 K. The x- and z-axis are in nm.

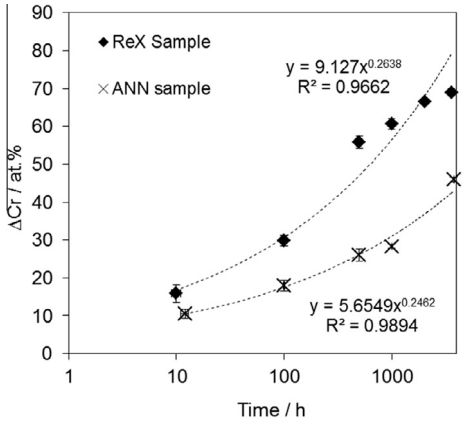

Fig. 3. The α–α′ phase separation during ageing at 748 K: comparison between Rex and ANN samples.

Fig. 3. The delay in the α–α′ phase separation kinetics shown in Fig. 3 might be twofold. Firstly, the thermal vacancies formed during homogenization annealing at 1623 K in ReX samples might recombine or form nanovoids instead, reducing the number of free vacancies able to boost the α–α′ phase separation kinetics. Therefore, an increase in the number density of nanovoids might be expected in ANN samples. Moreover, the thermal vacancies formed might diffuse away to the oxide particles. Oxides are a definite sink for vacancies and a preferential nucleation site for nanovoids. Therefore, the annealing treatment could induce, in fact, a reduction of thermal vacancies. These should lead to the formation of nanovoids in the interface between oxide particles and the matrix.

Secondly, that nanovoids and thermal vacancies present in the microstructure remain constant in terms of number density, but act as traps for solid solution elements such as Cr and/or Al.

An explanation to this apparent contradiction was investigated by PAS. PAS is a very powerful technique to investigate vacancy-type defects in metals because these defects are strong traps for thermal positrons in the crystal lattice. The PAS experiments were performed in a fast–fast coincidence spectrometer with a time resolution of 230 ps with the use of a ^{22}Na source sealed in kapton sandwiched between the pair of samples. Positron lifetime spectra with total count >10^6 were properly fitted to a sum of two lifetime components, τ_1 and τ_2, after subtracting the corrections due to positron annihilation in the ^{22}Na source. These spectra are characterized by a mean positron lifetime. The instrumental time resolution and contribution of the positron source to the lifetime spectra were determined from measurements on reference samples. Coincidence Doppler broadening (CDB) measurements were performed with two HP Ge detectors in timing coincidence, placed face to face with the samples at midpoint between the detectors. The resulting CDB spectrum was the cumulative spectrum of 24CDB spectra without evidence of electronic shift, each of them with a count number >10^6 in a 512×512 coincidence matrix. The cumulative spectra had 1×10^7 counts in the strip centered on the matrix diagonal for the energy range $2m_0c^2 - 1.6\ \text{keV} < E_1 + E_2 < 2m_0c^2 + 1.6\ \text{keV}$; E_1 and E_2 stand for the energies of the pair of annihilating photons, m_0 the electron rest mass and c the speed of light. The spectra were binned from 512 to 40 bins with a bin width of $2.5 \times 10^{-3}\ m_0c$ to decrease the statistical fluctuations of the data in the high momentum region. The spectra were then normalized and the intensity at a given photon momentum divided by the corresponding counts in the CDB spectrum of different reference samples in order to highlight the differences between the spectra.

Both, the ANN and ReX samples exhibited a two-component lifetime spectra characterized by short lifetime component of 120 ± 3 ps and long one of 300 ± 5 ps with intensity of 20 ± 2%. This lifetime component indicated the presence of tridimensional vacancy clusters, or nanovoids, which could consist of about 6 vacancies according to calculi for Fe [19,20].

It should be noticed that the respective contributions coming from annihilations in the small vacancy clusters and in Y-rich particles cannot be separated like Krsjak et al. [21] did for PM2000 using the decomposition approach applied by Vehanen et al. [22] for pure α-Fe. The ODS alloy PM2000 has a microstructure very complex to assume that the positron annihilation takes place in three possible positron states: Bloch positrons in the lattice, trapped in dislocation and trapped in vacancy clusters or/and Y-rich nanofeatures. In the ODS alloys there exist an abundant variety of defects than can be effective positron traps: impurity-vacancy defects, dislocations, second phase particles (oxides and carbides) in addition to nanofeatures associated to Y or Y_2O_3. Moreover, the assumption of a lifetime of ~240 ps attributable to annihilation in Y_2O_3 particles is rather misleading because experimental results have not been reported indicating that this lifetime value can be attributed to annihilation in the Y_2O_3 lattice. Damonte et al. [23] found that lifetime in Y_2O_3 powder but it was attributed to the superposition of annihilations from bulk lifetime and vacancy-like defects. We have performed measurements on Y_2O_3 nano-powders and single crystal in different conditions. These measurements resulted in a lifetime of ~230 ps that can be attributed to vacancy-like defects more consistently than to the Y_2O_3 bulk.

The fact these defects are stable at as high temperature as 1623 K suggests that they have to be associated with some impurities and/or alloying elements. Moreover, the coincidence in the intensity of the second lifetime component indicated that the ANN samples do not contain a significantly higher number density of the these vacancy type defects compared with the ReX samples, as it was expected. This is consistent with APT results that show a slower α–α′ kinetics.

Fig. 4 shows the CDB ratio spectra for sample ANN along with those for Fe, Al and Cr reference samples normalized to the CDB spectrum for the ReX sample. The ratio curve ANN sample is practically indistinguishable from Cr curve in the low momentum range ($P_L < 15 \times 10^{-3}\ m_0c$). This means that the positrons in the ANN sample annihilate with core electrons from Cr atoms. The ratio curve for ANN sample is also found below 1 but above the Cr curve for $P_L > 15 \times 10^{-3}\ m_0c$, this means that the positrons

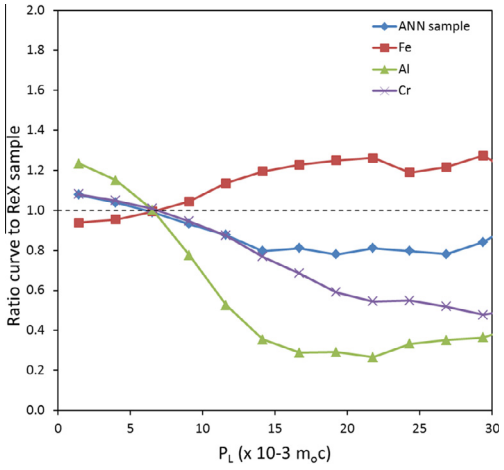

Fig. 4. CDB ratio spectra for ANN sample normalized to ReX sample.

Please cite this article in press as: C. Capdevila et al., Scripta Mater. (2015), http://dx.doi.org/10.1016/j.scriptamat.2015.07.044

mainly annihilate with core electrons from Fe (note that the shape of the curve is quite similar to that corresponding to Fe). The high concentration of Cr in the PM2000™ is responsible for the depletion in the high momentum region, compared to the Fe CDB spectrum. This is the expected effect for Cr in the Fe matrix. One concludes from this figure that annihilation of positrons trapped at defects occurs preferentially with Cr electrons, which indicated that chemical surrounding of the defects is Cr enriched compared with the matrix. Moreover, the comparison between the ratio curves to Cr for the ANN sample and for Al reveals no participation of Al atoms in the chemical surrounding of the defects.

The above, besides indicating the presence Cr atoms in the surrounding of the defects in the ANN samples, reveals a higher probability of positron annihilation events with Cr electron in the matrix compared with the ReX sample. These facts leads us to conclude that the vacancy type defects present in the microstructure of the ANN samples, like nanovoids detected by TEM in Fig. 1 and PAS, are found decorated with more Cr atoms than in the case of the ReX samples.

The present results are in contrast with the interpretation of the positron lifetime measurements made in PM2000, and other ODS FeCr alloys, with respect to the α' precipitation. Krsjak et al. [21] attribute the absence of α' particles in ODS Eurofer aged at 475 °C to vacancy agglomeration. This conclusion is achieved when the results from the ageing treatment for ODS Eurofer in the extruded condition are compared with those for ODM751 and PM2000 both in the recrystallized condition. For right comparisons, it is needed to start the isothermal ageing with samples in the same condition besides with the same Cr content. The precipitation of α' particles would more probable in PM2000 than in ODS Eurofer.

In summary, the presence of tridimensional vacancy complex defects and/or nanovoids inherent to the manufacturing route of ODS PM2000 can affect the α–α' phase separation in PM2000. Positron lifetime spectrum indicates that the number density of these defects remains practically the same in the Rex and ANN samples. These defects appear to be decorated with Cr as a result of the 1473 K quenching in contrast with the result for the samples annealed at 1623 K for 3 h, as CDB spectra reveal. So, Cr sinks into the preexisting vacancy clusters during annealing at 1473 K, and therefore, can lead to a significant decrease of Cr content in the matrix. This delays the kinetics of α–α' phase separation process as the APT reveal.

Acknowledgments

PM 2000™ is a trademark of Plansee GmbH. LEAP® is a registered trademark of CAMECA Instruments Inc. This research was supported by ORNL's Center for Nanophase Materials Sciences (CNMS), which is a U.S. Department of Energy, Office of Science User Facility. Authors acknowledge financial support to Ministerio de Economia (MINECO) and Fondo Europeo de Desarrollo Regional (FEDER) in the form of MAT2013-47460-C5-2-P project.

References

[1] V. de Castro, T. Leguey, A. Muñoz, M.A. Monge, P. Fernández, A.M. Lancha, R. Pareja, J. Nucl. Mater. 367–370 (2007) 196.
[2] Y. de Carlan, J.L. Bechade, P. Dubuisson, J.L. Seran, P. Billot, A. Bougault, T. Cozzika, S. Doriot, D. Hamon, J. Henry, M. Ratti, N. Lochet, D. Nunes, P. Olier, T. Leblond, M.H. Mathon, J. Nucl. Mater. 386–388 (2009) 430.
[3] S. Ukai, M. Harada, H. Okada, M. Inoue, S. Nomura, S. Shikakura, K. Asabe, T. Nishida, M. Fujiwara, J. Nucl. Mater. 204 (1993) 65.
[4] G. Bonny, D. Terentyev, L. Malerba, J. Phase Equilib. Diff. 31 (2010) 439.
[5] S. Novy, P. Pareige, C. Pareige, J. Nucl. Mater. 384 (2009) 96.
[6] C. Capdevila, Y.L. Chen, N.C.K. Lassen, A.R. Jones, H.K.D.H. Bhadeshia, Mat. Sci. Technol. 17 (2001) 693.
[7] D.M. Jaeger, A.R. Jones, in: Proc. Conf. Materials for Combined Cycle Power Plant, 1991, London, pp. 1–11.
[8] C. Capdevila, U. Miller, H. Jelenak, H.K.D.H. Bhadeshia, Mater. Sci. Eng., A 316 (2001) 161.
[9] C. Capdevila, H.K.D.H. Bhadeshia, Adv. Eng. Mater. 3 (2001) 647.
[10] V. de Castro, T. Leguey, M.A. Auger, S. Lozano-Perez, M.L. Jenkins, J. Nucl. Mater. 417 (2011) 217.
[11] C.M. Parish, M.K. Miller, Microsc. Microanal. 20 (2014) 613.
[12] Y. Ortega, M.A. Monge, V. de Castro, A. Muñoz, T. Leguey, R. Pareja, J. Nucl. Mater. 386–388 (2009) 462.
[13] R. Pareja, P. Parente, A. Muñoz, A. Radulescu, V. de Castro, Phil. Mag. (2015) 1–16.
[14] M.K. Miller, Atom Probe Tomography, Kluwer Academic/Plenum Press, New York, NY, 2000.
[15] M.K. Miller, J.M. Hyde, M.G. Hetherington, A. Cerezo, G.D.W. Smith, C.M. Elliott, Acta Metall. Mater. 43 (1995) 3385.
[16] O.C. Hellman, J.A. Vandenbroucke, J. Rüsing, D. Isheim, D.N. Seidman, Microsc. Microanal. 6 (2000) 437.
[17] I.M. Lifshitz, V.V. Slyozov, J. Phys. Chem. Solids 19 (1961) 35.
[18] C. Wagner, Z. Elektrochem. 65 (1961) 581.
[19] H. Ohkubo, Z. Tang, Y. Nagai, M. Hasegawa, T. Tawara, M. Kiritani, Mater. Sci. Eng., A 350 (2003) 95–110.
[20] J. Kuriplach, O. Melikhova, C. Domain, C.S. Becquart, et al., Appl. Surf. Sci. 252 (2006) 3303–3308.
[21] V. Krsjak, Z. Szaraz, P. Hähner, J. Nucl. Mater. 428 (2012) 160–164.
[22] A. Vehanen, P. Hautojärvi, J. Johansson, J. Yli-Kauppila, P. Moser, Phys. Rev. B 25 (1982) 762–780.
[23] L.C. Damonte, M.A. Taylor, J. Desimoni, J. Runco, Radiat. Phys. Chem. 76 (2007) 248.